HAL
archives-ouvertes.fr

Model to interpret pulsed-field-gradient NMR data including memory and superdispersion effects.

Marie-Christine Néel, Daniela Bauer, Marc Fleury

▶ **To cite this version:**

Marie-Christine Néel, Daniela Bauer, Marc Fleury. Model to interpret pulsed-field-gradient NMR data including memory and superdispersion effects.. Physical Review E : Statistical, Nonlinear, and Soft Matter Physics, American Physical Society, 2014, 89 (6), pp.No 062121. <10.1103/PhysRevE.89.062121>. <hal-01052931>

HAL Id: hal-01052931

https://hal-ifp.archives-ouvertes.fr/hal-01052931

Submitted on 29 Jul 2014

HAL is a multi-disciplinary open access archive for the deposit and dissemination of scientific research documents, whether they are published or not. The documents may come from teaching and research institutions in France or abroad, or from public or private research centers.

L'archive ouverte pluridisciplinaire **HAL**, est destinée au dépôt et à la diffusion de documents scientifiques de niveau recherche, publiés ou non, émanant des établissements d'enseignement et de recherche français ou étrangers, des laboratoires publics ou privés.

A model to interpret pulsed field gradient NMR data, including memory and super-dispersion effects

Marie-Christine Néel,[1,*] Daniela Bauer,[2,†] and Marc Fleury[2,‡]

[1] *Université d'Avignon et des Pays de Vaucluse,*
UMR 1114 EMMAH, F-84018 Avignon Cedex, France

[2] *IFP Energies nouvelles, 1 et 4, avenue de Bois Préau 92852 - Rueil-Malmaison, France*

Abstract

We propose a versatile model specifically designed for the quantitative interpretation of NMR velocimetry data. We use the concept of Mobile/ Immobile tracer particles applied in dispersion theory in its Lagrangian form, adding two mechanisms: (i) independent random arrests of finite average representing intermittent periods of very low velocity zones in the mean flow direction and (ii) the possibility of unexpectedly long (but rare) displacements simulating the occurrence of very high velocities in the porous medium. Based on mathematical properties related to subordinated Lévy processes, we give analytical expressions of the signals recorded in pulsed field gradient NMR experiments. We illustrate how to use the model for quantifying dispersion from NMR data recorded for water flowing through a homogeneous grain pack column in single and two phase flow conditions.

PACS numbers: 05.40.Fb, 02.50.Ey, 47.56.+r

*Electronic address: mcneel@avignon.inra.fr

†Electronic address: daniela.bauer@ifpenergiesnouvelles.fr

‡Electronic address: marc.fleury@ifpenergiesnouvelles.fr

I. INTRODUCTION

Solute migration in porous materials results from random molecular motions superimposed to highly complex pore scale velocity field [1]. Commonly, it is characterized by tracer tests together with various dispersion models in order to reproduce concentration profiles. With the same objective, the pulsed field gradient (PFG) NMR technique, although not new, is becoming more and more popular. Indeed, it is a non-intrusive measurement method providing a unique insight into molecular motion statistics without the need of any tracer [2]. More specifically, pulsed field gradient NMR velocimetry typically records signals proportional to the characteristic function $\langle e^{-ik\Delta x}\rangle$ of water molecule displacements Δx in the mean flow direction (as studied by most authors, but any other direction is also possible). Commonly, such signals are usually Fourier transformed into propagators (distribution of displacements) and their shape analyzed. Alternatively, the empirical moment of order two (or up to three) can also be calculated directly from the signal, but such functional does not allow discriminating sometimes dramatically different stochastic processes [3]. With such capabilities, the PFG-NMR technique gives crucial information for stochastic models, but to our knowledge, no in-depth interpretation of NMR signals is available in literature. Here, we are seeking a versatile model and numerical tool that can reproduce standard Gaussian dispersion as well as non-Gaussian effects that are observed in heterogeneous porous samples [4], or in homogeneous samples but in two phase flow conditions [5]. Non-symmetric shapes of propagators do not necessarily mean anomalous dispersion because an asymptotic regime may not be reached when analyzing short time data. Nevertheless, assessing the onset of asymptotic behaviors motivates studying shorter displacements as well, by applying very accurate numerical or experimental methods available at small scales [6][7]. Finally, another important feature of our approach is to avoid the difficulties related to Fourier transforms and calculate the model parameters directly from the PFG-NMR signals.

Two main features are present in the non-Gaussian propagators represented in [4] and [5]: non-symmetric shapes with a tail at large displacements, and in some cases small peaks or humps present around zero displacement, suggesting that some molecules may be stacked in non flowing zones in the porous media. Fig. 1 displays some examples discussed in [5] and measured in a porous column as summarized in Appendix A. Asymmetric propagators disagree with any Gaussian model, even associated to time-dependent second moment as

stretched Brownian motion [8]: most propagators portrayed on Fig. 1 are reminiscent of stable process, whose displacement distribution is easy to describe. However, stable processes do not account for small humps as on Fig. 1 (right) for $\Delta t = 0.1s$. We account for such features as well as for propagators showing peaks [4] by means of a random time change based on two independent sequences M_n (mobile) and W_n (immobile), representing time lapses during which a Lévy motion is alternatively turned on and off. Using such time schedule is supported by Lagrangian simulations of Navier-Stokes equations between obstacles, evidencing intermittent time lapses during which fluid particles take very low velocities [9]. Since we do not observe propagators showing tall peaks, we disregard pausing times of infinite mean [10], and choose exponentially distributed M_n and W_n [11]. The influence of each such sequence is summarized by a random time change replacing clock time t by the operational time Z_t [12] that sums up all mobile periods elapsed before. Such time change returns non-symmetric propagators by its own, even when applied to Gaussian or more general stable symmetric processes. This suggests comparing NMR signals with stochastic processes deduced from general Lévy motions ([13, 14]) by applying the random time change: the immobile time sequence W_n attempts representing the time each molecule spends in non-flowing zones in the porous media, or displacements in the transverse direction to the mean flow. We demonstrate how such comparison applies to experimental NMR signals.

The proposed model also includes existing ones. Indeed, applying the above time schedule to any stable process X_t yields a new process X_{Z_t} that belongs to the wide set of subordinated Lévy motions. In the particular case when X_t is Gaussian, X_{Z_t} coincides with the stochastic version [11, 15, 16] of the Mobile-Immobile Model (MIM), [1, 17–19] used to describe tracer dispersion in natural porous materials. MIM accounts for tracer particles that can be found in two states, mobile and immobile. It consists of a mass conservation equation based on Fickian fluxes deduced from the density of mobile particles, while exchanges with the immobile fluid fraction being described by first order kinetics. In the more general case of any stable process X_t , X_{Z_t} represents the motions of walkers that follow the sample pathways of its parent X_t, but are found at location X_{Z_t} instead of X_t, at clock time t. Thus associating a stable process to MIM's operational time yields a wide class of models that contains the stochastic analogue of the classical MIM: following [11] we call its elements stochastic Mobile Immobile Models, noted SMIM. Since X_{Z_t} is a subordinated process, it is not Markovian,

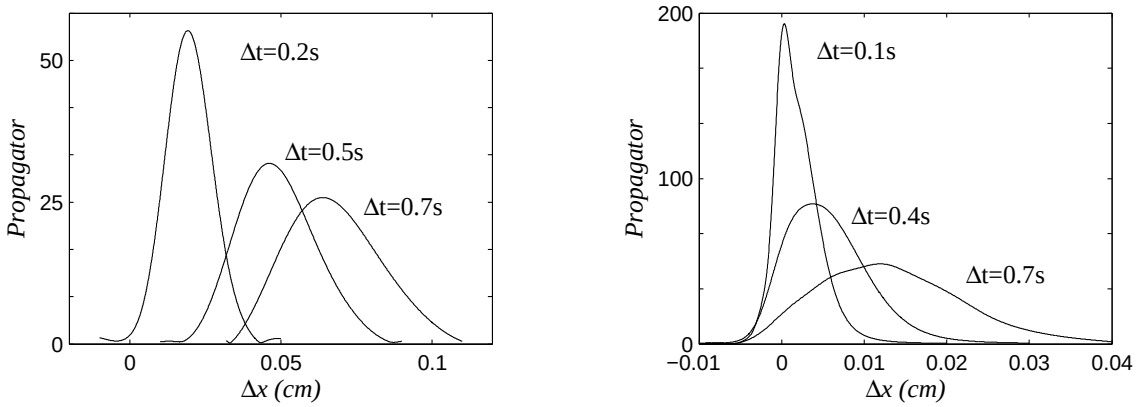

FIG. 1: Example of NMR propagators measured in a $30\mu m$ grain pack column [5] in single phase flow (left) and two phase flow conditions (right). Note the non symmetric shape especially obvious in two phase flow conditions

and the distribution of its increments [20] is not so simple as for the parent or for any system with independent increment as in [8]. However, the operational time Z_t is the hitting time of a compound Poisson process (CPP), an increasing process with independent increments [21]. Taking advantage of this, we compute exactly the increment characteristic function of X_{Z_t}. Hence, we have a direct and quantitative comparison with NMR experiments that sample function $\langle e^{-ik\Delta x}\rangle$, and this will prove very useful when calculating the model parameters from NMR data using inversion methods. Moreover, applying later this approach to any Lagrangian description of dispersion [22–26] will be very easy, and permit comparisons between models.

We first remind how the SMIM is deduced from a stable parent process by changing its time schedule. Then, the characteristic function of SMIM's displacements is given an analytical expression based on probabilistic arguments, corroborated by numerical proof. Finally, we demonstrate how we use the analytical expression for inverting laboratory NMR signals recorded in a sand column in single and two phase flow conditions.

II. THE STOCHASTIC MOBILE-IMMOBILE MODEL

We describe here two essentials of the SMIM, i.e. stable process and time schedule.

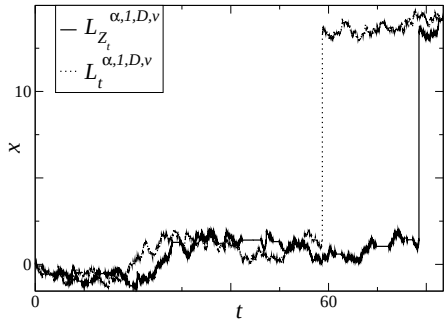

FIG. 2: Sample paths of the SMIM, and of its parent process. Dotted and full lines represent trajectories of stable parent $L_t^{\alpha,1,D,v}$ and subordinated process $L_{Z_t}^{\alpha,1,D,v}$, for $\alpha = 1.7$, $D = 0.1$, $v = 0.1$, $K = 0.5$ and $\omega = 1$ (ω and K being defined in Subsection II B).

A. Stable processes

Stable processes [13, 14] generalize Brownian motion, but include skewness and possibly diverging second (and even first) order moments. As for Gaussian processes, each stable process $L_t^{\alpha,\beta,D,v}$ has independent stationary increments (i.e. is a Lévy process [21]): for each $dt > 0$, $L_{t+dt}^{\alpha,\beta,D,v} - L_t^{\alpha,\beta,D,v}$ is distributed ($\stackrel{d}{=}$) as the right hand side of

$$L_{t+dt}^{\alpha,\beta,D,v} - L_t^{\alpha,\beta,D,v} \stackrel{d}{=} vdt + (Ddt)^{\frac{1}{\alpha}}\mathcal{L}^{\alpha,\beta}, \tag{1}$$

the stable random variable $\mathcal{L}^{\alpha,\beta}$ being briefly described in Appendix B (with $\alpha \in]0, 2]$ and $\beta \in [-1, 1]$). When the stability exponent α takes its maximal value 2, $\mathcal{L}^{2,\beta}$ is exactly a normal variable, $L_t^{2,\beta,D,v}$ is a Gaussian process, and the value of β has no influence. Otherwise non-zero β values correspond to skewed p.d.fs represented in Appendix B. For $\alpha > 1$, the mathematical expectation of $\mathcal{L}^{\alpha,\beta}$ is equal to zero (otherwise it is infinite). In this case, which attracts our attention, $L_t^{\alpha,\beta,D,v}$ describes individual motions of walkers of average velocity v. Parameter D is a scale factor of dimensionality $\frac{[L]^\alpha}{[T]}$, generalizing the usual diffusivity or dispersion in the Gaussian case ($\alpha = 2$). We will use the characteristic function $\langle e^{-ikL_t^{\alpha,\beta,D,v}}\rangle = e^{-t(ikv+D\varphi_{\alpha,\beta}(k))}$, whose exponential rate $\varphi_{\alpha,\beta}$ is detailed in Appendix B: due to (1) , $L_{t_1+\Delta t}^{\alpha,\beta,D,v} - L_{t_1}^{\alpha,\beta,D,v}$ has a characteristic function equal to $e^{-\Delta t(ikv+D\varphi_{\alpha,\beta}(k))}$, for each pair $(t_1, \Delta t)$ of positive numbers.

SMIM's sample paths are deduced from those of any stable process $L_t^{\alpha,\beta,D,v}$ by applying the random time change Z_t defined below: this means that we consider walkers whose location at time t is described by $L_{Z_t}^{\alpha,\beta,D,v}$ instead of $L_t^{\alpha,\beta,D,v}$, as on Fig. 2.

B. Random time change accounting for pausing times of finite average

We define here the operational time Z_t that describes the evolution of the accumulated mobile time along sample sequences (M_n, W_n) of successive independent mobile and immobile steps, which define the classical MIM. Then, we briefly recall mathematical properties linking Z_t to an other process $(T(z))$ that helps us describing the increments of the former, which are neither independent, nor stationary.

In the SMIM as in the MIM, each walker performs random motions restricted to time intervals whose lengths form a sequence M_n [11], each of them being followed by a random pausing time W_n. These variables are mutually independent, with exponential distributions of average $\frac{1}{K\omega}$ for the M_n, and $\frac{1}{\omega}$ for the W_n: parameter K is the average rest time divided by the average mobile time. Moreover, the M_n and W_n are independent of the stable parent $L_t^{\alpha,\beta,D,v}$. Inserting a pause of duration W_n between each two successive intervals of length M_n and M_{n+1} yields a process, whose each time t value depends on the total amount of time Z_t spent moving before that instant. More specifically, on each sample path of the (M_n, W_n) sequence the operational time Z_t takes a value entirely determined by the sample path itself, and by t, as follows. If we call this value z, it is $z = M_1 + ... + M_n$ if the walker is immobile at time instant t. During the mobile time interval of rank $n+1$, by contrast, z satisfies $z = M_1 + ... + M_n + \theta$ with $0 < \theta < M_{n+1}$: $\theta = 0$ at the beginning of the current mobile period, and $\theta = M_{n+1}$ at its end. In between, θ is equal to the increase of clock time t since period began. Square and circle mark time instants realizing first and second possibility respectively, on Fig. 3. This defines process Z_t itself. In view of being able to describe its increments (neither independent nor stationary), we now relate it to another process that has independent stationary increments.

At each stage, the number of mobile steps completed when Z_t takes the value z is equal to the largest integer i satisfying $M_0 + ... + M_i \leq z$, where we set $M_0 = W_0 = 0$ for convenience. Since the M_i (except M_0) are exponentially distributed, this number is given by $N(z)$, a Poisson process of rate $K\omega$: it takes each integer value n with probability $\mathcal{P}\{N(z) = n\} = e^{-\omega K z}\frac{(K\omega z)^n}{n!}$. All information concerning each value z of Z_t is deduced from another process that we note T [11], defined by

$$T(z) \equiv z + W_0 + ... + W_{N(z)}. \tag{2}$$

It is a Compound Poisson process (CPP): it has independent increments, and is strictly

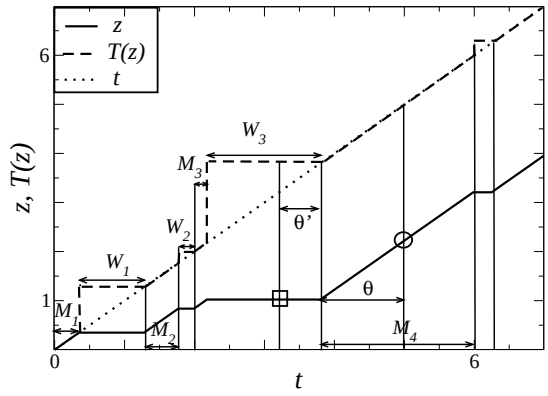

FIG. 3: The values z and $T(z)$ of the operational time Z_t and of the subordinator, on a sample path of the sequence of mobile/immobile steps of the MIM. The time instant marked by a square belongs to the immobile step of rank $n = 3$, during which z, $N(z)$ (equal to n) and $T(z)$ are necessarily constant, whereas t increases continuously: $T(z)$ then represents the clock time of the end of the current step. The time point marked by a circle belongs to the immediately following mobile step, in the course of which z increases continuously, $N(z)$ keeping its value n, while $T(z)$ (defined by Eq. (2)) coincides with the clock time t. At the end of this step, i.e. when z passes $M_0 + ... + M_n + M_{n+1}$, $N(z)$ and $T(z)$ suddenly increase by 1 and W_{n+1}, respectively.

increasing (hence we call it a Lévy subordinator) [21]. It is characterized by its Laplace transform $\langle e^{-sT(z)} \rangle = e^{-z\psi(s)}$, with $\psi(s) = s(1 + \frac{K\omega}{s+\omega})$.

On each sample path (as the one represented on Fig. 3), the operational time Z_t satisfies

$$Z_t = \inf \{ y / T(y) > t \} , \tag{3}$$

meaning that Z_t is the hitting time of $T(z)$ [11]. Associating Eq. (3) to the fact that $T(z)$ is a Lévy subordinator will give us almost for free (in Section III) the increment characteristic function of Z_t, and of the SMIM, equal to parent process computed operational time Z_t.

C. SMIM's trajectories

For each realization of the sequence (M_n, W_n), each sample path of the parent $L_t^{\alpha,\beta,D,v}$ gives one sample path of $x_t = L_{Z_t}^{\alpha,\beta,D,v}$. The (M_n) sequence divides the parent trajectory into segments $I_n \equiv \left\{ (\theta, L_\theta^{\alpha,\beta,D,v}) / \sum_{i=0}^{n-1} M_i \leq \theta < \sum_{i=0}^{n} M_i \right\}$, limited by "$\times$" symbols on Fig. 4. Due to delays $W_0, ..., W_{n-1}$, the mobile interval of rank n (≥ 1) of the SMIM trajectory is

deduced from I_n by applying the time shift $S_{\Omega_{n-1}}$ of amplitude $\Omega_{n-1} \equiv W_0 + ... + W_{n-1}$: shifted copies $S_{\Omega_{n-1}}(I_n)$ are limited by diamonds on the trajectory of x_t represented on Fig. 4. Each $S_{\Omega_{n-1}}(I_n)$ is immediately followed by an immobile step I'_n, of duration W_n, during which x_t stays fixed at $L^{\alpha,\beta,D,v}_{M_0+...+M_n}$. Of course, we have $S_{\Omega_0}(I_1) = I_1$, and the complete trajectory of x_t is the union of all $S_{\Omega_{n-1}}(I_n)$ and I'_n.

D. SMIM's p.d.f.

The above description of the SMIM allows us using tools developed within Continuous Time Random Walk (CTRW , see [27, 28]) framework. The SMIM is a correlated CTRW ([29]), since walkers perform random motions not independent of the time lapses during which they occur. Adapting CTRW tools to describe walkers that can be found in mobile or immobile state, one retrieves the densities given in [11] for these two populations. One thus shows that the p.d.f. $P(x,t)$ of x_t satisfies

$$\partial_t P + K\omega e^{-\omega t} * \partial_t P = \mathcal{A}P, \tag{4}$$

with

$$\mathcal{A}P(x,t) \equiv \partial_x[-vP] - \frac{D}{2\cos\frac{\pi\alpha}{2}}[(1+\beta)D^{\alpha}_{-\infty,x} + (1-\beta)D^{\alpha}_{x,+\infty}]P,$$

derivatives $D^{\alpha}_{-\infty,x}$ and $D^{\alpha}_{x,+\infty}$ (of order α) being defined in Appendix C for $\alpha < 2$: in the limit case $\alpha = 2$, $\mathcal{A}$ becomes $-v\partial_x + D\partial^2_{x^2}$, and (4) is the classical version of the MIM.

Eq. (4) would be very useful to interpret tracer tests, with concentration instead of P. Here, we consider different observables.

E. SMIM's propagators

SMIM's increments distributions are easily described by means of random walks combining temporal disorder and Lévy motion (the latter including the Gaussian case). For each sample sequence (M_i, W_i), operational times $Z_{t_1+\Delta t}$ and Z_{t_1} are determined as in Subsection II B. Drawing independent copies of $\mathcal{L}^{\alpha,\beta}$ then samples displacements $x_{t_1+\Delta t} - x_{t_1}$, distributed as $v(Z_{t_1+\Delta t} - Z_{t_1}) + (D(Z_{t_1+\Delta t} - Z_{t_1}))^{\frac{1}{\alpha}}\mathcal{L}^{\alpha,\beta}$ due to (1). Histograms of the latter approximate propagators.

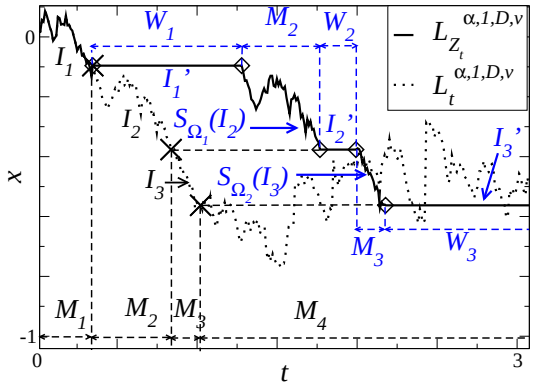

FIG. 4: Mobile and immobile steps of a sample path of the SMIM. The figure is a magnification of the three first mobile steps of the sample path of $L_{Z_t}^{\alpha,1,D,v}$ (full line) whose global view is displayed on Fig. 2. They are deduced from successive segments of a sample path of the parent process (dotted line), by applying time shifts dictated by the arrest durations represented on Fig. 3. These durations determine the length of each plateau connecting two successive mobile steps. Only the first mobile step of the subordinated trajectory coincides with a segment of that of its parent.

Fig. 5 displays examples of thus obtained propagators: some of them resemble pictures represented on Fig. 1. Others show peaks as on Fig. 1-b. of [4]. Values of α smaller than 2 yield non-symmetric shapes, provided $\beta \neq 0$. Large K values yield peaks (especially when t_1 is large) that result into skewness even with $\alpha = 2$. Nevertheless, such peaks fade out when Δt is increased: in fact, only skewness caused by $\alpha < 2$ and $\beta \neq 0$ remains at large Δt, though it is not obvious on figures representing several propagators as Fig. 5, because of scale effects.

The visual analogy with experimental propagators motivated our interest in the SMIM. Yet, featuring propagators necessitates inverse Fourier transform, which causes a lot of approximations and errors that we avoid by directly comparing NMR signal with increment characteristic function of model.

III. THE CHARACTERISTIC FUNCTION OF THE INCREMENTS OF THE SMIM

For such comparison, we derive a closed form expression for the characteristic function of the increments of x_t. Such expression is much more comfortable to handle than a p.d.e,

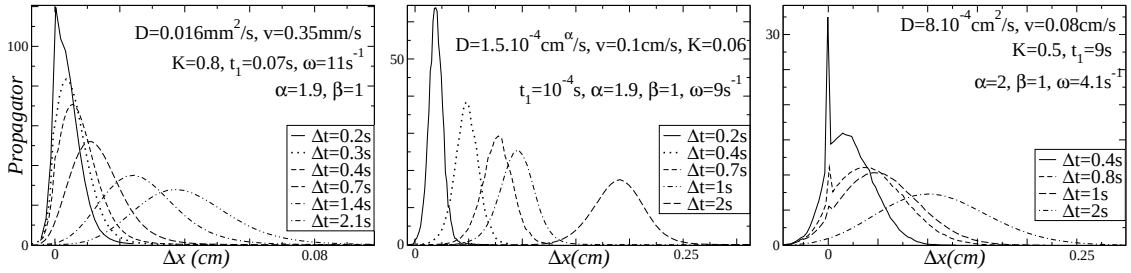

FIG. 5: Some examples of propagators, deduced from the SMIM with $\beta = 1$. Some of them resemble experimental propagators of Fig. 1, and we also observe a propagator showing a peak, reminiscent of Figure 1.b of [4]. For all parameter values, streaking features observed at small displacement duration Δt become less visible when this quantity is increased.

and allows us using efficient optimization to guess SMIM's parameters that fit experimental data. Because Z_t and $L_t^{\alpha,\beta,D,v}$ are independent, the characteristic function $\langle e^{-ik[x_{t_1+\Delta t}-x_{t_1}]}\rangle$ of $x_{t_1+\Delta t} - x_{t_1}$ is deduced from the Laplace transform $\langle e^{-\eta[Z_{t_1+\Delta t}-Z_{t_1}]}\rangle$ of $Z_{t_1+\Delta t} - Z_{t_1}$. Its mathematical expression will confirm trends noticed in section II E, regarding the influence of K and Δt.

A. From the characteristic function of $Z_{t_1+\Delta t} - Z_{t_1}$ to that of $x_{t_1+\Delta t} - x_{t_1}$

Indeed, process $L_t^{\alpha,\beta,D,v}$ having independent increments, conditioning on the value of $Z_{t_1+\Delta t} - Z_{t_1}$ shows that the characteristic function $\langle e^{-ik[x_{t_1+\Delta t}-x_{t_1}]}\rangle$ of x_t is exactly

$$\langle e^{-ik[x_{t_1+\Delta t}-x_{t_1}]}\rangle = \langle e^{-\eta[Z_{t_1+\Delta t}-Z_{t_1}]}\rangle,$$

with $\eta = ikv + D\varphi_{\alpha,\beta}(k)$ [30, 31]. Now, it turns out that the Laplace transform $\langle e^{-\eta[Z_{t_1+\Delta t}-Z_{t_1}]}\rangle$ of $Z_{t_1+\Delta t} - Z_{t_1}$ has an analytical expression (D4), detailed in Appendix D. This implies

$$\langle e^{-ik[x_{t_1+\Delta t}-x_{t_1}]}\rangle = F(\alpha, \beta, v, D, \omega, K, e^{-\omega(K+1)t_1}, k, \Delta t) \tag{5}$$

with

$$F(\alpha, \beta, v, D, \omega, K, \mathcal{M}, k, \Delta t) \equiv \tfrac{\eta}{K+1} \times [(H_- + G\mathcal{M})e^{r_-\Delta t} - (H_+ + G\mathcal{M})e^{r_+\Delta t}], \tag{6}$$

functions $r_\pm$, $H_\pm$ and G (of $\alpha, \beta, v, D, \omega, K$) being defined in Appendix D. Eq. (5) is demonstrated by Fig. 6, which compares $F(\alpha, \beta, v, D, \omega, K, e^{-\omega(K+1)t_1}, k, \Delta t)$ with Monte Carlo simulations of $\langle e^{-ik[x_{t_1+\Delta t}-x_{t_1}]}\rangle$.

Because of the time change, $L_{Z_t}^{\alpha,\beta,D,v}$ is not a Markovian process: we see from (5) that the distribution of its increments is influenced by t_1, the age of each walker when displacements begin being measured. It coincides with clock time if all walkers start at a given time origin. In numerical experiments, we easily impose a common time origin to all walkers. Real experiments, differently, record displacements of molecules that may have been launched in the device at different times: then, t_1 must be regarded as a random variable instead of a deterministic parameter, especially when walkers are fluid molecules in an open flow experiment.

B. Walker age distribution

In general, instead of $\langle e^{-ik[x_{t_1+\Delta t}-x_{t_1}]}\rangle$ we measure

$$\langle e^{-ik\Delta x}\rangle = \int_0^{+\infty}\langle e^{-ik[x_{t_1+\Delta t}-x_{t_1}]}\rangle p(t_1)dt_1, \tag{7}$$

$p(t_1)$ being the fraction of walkers of age t_1 in the population of particles whose displacements are actually recorded. Though we may have few information on p, t_1 is only involved in the item $\mathcal{M} = e^{-\omega(K+1)}$ of (6), and we still have

$$\langle e^{-ik\Delta x}\rangle = F(\alpha,\beta,v,D,\omega,K,\mathcal{M},k,\Delta t), \tag{8}$$

provided we set

$$\mathcal{M} = \int_0^{+\infty} e^{-\omega(K+1)t_1}p(t_1)dt_1 \tag{9}$$

instead of $\mathcal{M} = e^{-\omega(K+1)t_1}$ that holds when p is a Dirac atom, as when all walkers start the random walk at the same time origin. Even if we do not know function p in practice, the parameter $\mathcal{M}$ involved in (8) can be deduced from $\langle e^{-ik\Delta x}\rangle$ records, as other parameters.

C. The behavior of $F(\alpha,\beta,v,D,\omega,K,\mathcal{M},k,\Delta t)$ when Δt and K are varied

Experimental propagators displayed on Fig. 1 correspond to parameter values satisfying $\omega > 1 > K$, D and v being small. With such parameters and with $\eta = ikv + D\varphi_{\alpha,\beta}(k)$, wave numbers k that are not too large satisfy $\frac{|\eta|}{\omega(K+1)} << 1$: according to Appendix D, $F(\alpha,\beta,v,D,\omega,K,\mathcal{M},k,\Delta t)$ is dominated by an expression proportional to $e^{-\Delta t\frac{D\varphi_{\alpha,\beta}+ikv}{K+1}}$ when Δt is large. One thus obtains signals very close to those of stable process $L_t^{\alpha,\beta,\frac{D}{K+1},\frac{v}{K+1}}$,

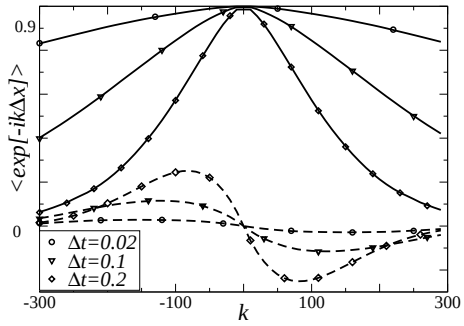

FIG. 6: Numerical demonstration of (5). Monte Carlo simulation of $\langle e^{-ik[x_{t_1+\Delta t}-x_{t_1}]}\rangle$ (symbols) are obtained in two steps. Step 1 consists in sampling Z_{t_1} and $Z_{t_1+\Delta t}$ by drawing sequences M_n and W_n, which yields the z values corresponding to clock times t_1 and $t_1+\Delta t$, as for Fig. 3. Step 2 then uses (1) with $dt = Z_{t_1+\Delta t} - Z_{t_1}$ to sample $x_{t_1+\Delta t} - x_{t_1}$. The thus obtained characteristic function coincides with $F(\alpha, \beta, v, D, \omega, K, e^{-\omega(K+1)}, k, \Delta t)$ (lines), whose real/imaginary part is represented by solid/dashed line. Parameters are $(\alpha, \beta, v, D, \omega, K, t_1) = (1.6, 1, 0.025, 0.001, 1000, 0.0001, 2)$

provided $\frac{|\eta|}{\omega(K+1)}$ is small. We only have a tight approximation, not a limit, and this results into SMIM propagators (as on Figs 9 and 11) resembling the p.d.f. of a stable random variable (see Fig. 13) when Δt is increased.

Decreasing to zero the immobile time per mobile time (K), differently, makes the SMIM tend to a stable process: for each fixed $(k, t_1, \Delta t)$, $F(\alpha, \beta, v, D, \omega, K, \mathcal{M}, k, \Delta t)$ tends to the characteristic function $e^{-\Delta t[D\varphi_{\alpha,\beta}(k)+ivk]}$ of $L_{\Delta t}^{\alpha,\beta,D,v}$ when $K \to 0$ if, moreover, $K\omega$ remains finite.

Beyond featuring these general trends, exact expression (8) gives us the opportunity of finding the parameters of SMIM model that allow it representing at best any rich enough given set of experimental data.

IV. COMPARING DATA AND SMIM

We first describe an inversion method for obtaining parameters $(\alpha, \beta, v, D, \omega, K, \mathcal{M})$. Then, we show the results using data previously published in [5] in single and two phase flow conditions, in the same grain pack. The single phase flow conditions indicate a slight super-dispersion behavior in the quasi-asymptotic regime, while for the two phase flow conditions,

propagators are more obviously non-Gaussian.

A. Principle of an inverse method for displacements characteristic function

The NMR signal $S(k, \Delta t)$ representing the characteristic function $\langle e^{-ik\Delta x} \rangle$ of displacements Δx during a series of time lapses of durations $\Delta t^{(m)}$ is acquired at discrete values $k_n^{(m)}$ (signals recorded for different $\Delta t^{(m)}$ may be acquired at different wave numbers). To find the best parameters fitting the data, we build an objective function E equivalent to the squared deviation between analytical characteristic function $F(\alpha, \beta, v, D, \omega, K, \mathcal{M}, k_n^{(m)}, \Delta t^{(m)})$ and data $S(k_n^{(m)}, \Delta t^{(m)})$, and find its minimum using standard optimization routine [32]. However, the optimization is performed in two steps: the objective function E is first minimized w.r.t. parameters $(v, D, \omega, K, \mathcal{M})$ for a fixed set of (α, β) values, returning a partial minimum $E_{min}^{\alpha,\beta}$. Then, the above minimization is repeated for different (α, β) values, and the overall minimum of all the $E_{min}^{\alpha,\beta}$ gives the best (α, β) values. For example, the curve shown in Fig. 7 indicates an overall minimum of E around 1.91 when $\beta = 1$. With the data analyzed here, we found that the overall minimum of E is always achieved for $\beta = 1$. Moreover, we normalized E with $\sigma^2 = \Sigma_{n,m}(|S(k_n^{(m)}, \Delta t^{(m)})| - |S(-k_n^{(m)}, \Delta t^{(m)})|)^2$, a lower bound of measurement errors since the modulus of any characteristic function must be an even function of the wave-number.

In the inversion method described above, it is important to take into account several NMR signals at different time durations Δt, because parameters K and ω reflect the influence of Δt. In addition, since the derivatives of E w.r.t. $v, D, \omega, K, \mathcal{M}$ are deduced analytically from Eq. (6), the occurrence of local minima is severely reduced compared to finite difference calculations. It is also a very fast calculation without any limit on the number of time durations that can be considered. Note also that we let the parameter $\mathcal{M}$ depend on Δt rather than being unique for the entire data set, because the population of walkers present in the measurement volume during a time interval of length Δt may be influenced by this quantity.

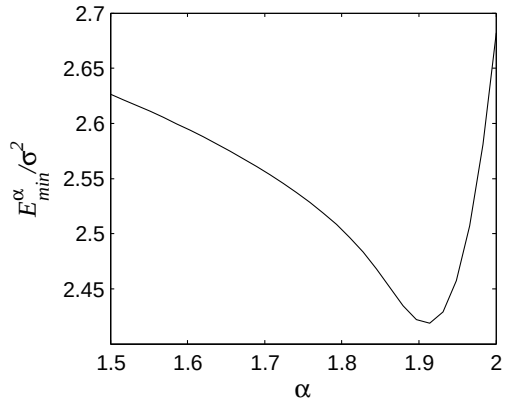

FIG. 7: The SMIM based normalized objective function E/σ^2 for a range of stability exponent (single phase flow conditions). The overall minimum of E is reached at $\alpha = 1.91$ ($\beta = 1$). Other optimized parameters are $D = 1.5 \times 10^{-4} cm^{\alpha}/s$, $v = 0.101 cm/s$, $\omega = 10.4 s^{-1}$, $K = 0.05$.

B. Using SMIM to characterize dispersion in porous media

We use the inversion method described above to analyze experiments performed in a $30\mu m$ grain pack of uniform porosity 0.42 [5]. The flow is performed in a long column but only a slice located in the middle is probed. We concentrate our attention on two series of signals, recorded either in single phase, or in two-phase flow conditions.

Single phase flow- In single phase flow conditions first, the data considered were collected at a flow rate of $700 ml/h$ and time duration Δt up to $1s$ (see Fig. 7 in reference [5]). However, at short time or short average displacement $\langle \Delta x \rangle$ compared to grain size d_g, displacement distributions are signatures of a pre-asymptotic regime in which the flow field around the grains and diffusion play an important role, as described by [6] and observed by [7]. Hence, we concentrate our attention on NMR data acquired in the quasi-asymptotic regime such as $\langle \Delta x \rangle / d_g > 10$, corresponding to time duration $\Delta t > 0.4s$. The experimental data points can be fitted with great accuracy (Fig. 8). Indeed, the normalized objective function based on all time durations above $0.4s$ (6 values) has a minimum of 2.4 (Fig. 7), i.e. the error between the model and the data is only 2.4 times the lower error bound σ^2. Using signals acquired at $\Delta t < 0.4s$ significantly rises the objective function E. By contrast, restricting the set of signals involved in the optimization process by removing data at Δt between $0.4s$ and $\Delta t^{(1)}$ yields estimated α values that remain constant when $\Delta t^{(1)}$ is increased, provided we still consider several displacement times. We mentioned above that

the latter condition is necessary for a robust parameter estimation. Note that we use general stable laws to build a model for small-scale motions. Since we have data with very small noise, Fig. 7 shows that restricting the model to the particular Gaussian case $\alpha = 2$ would increase the objective function. This confirms the slight super-dispersion suggested by [5], not revealed by a simple look at propagator shape (Fig. 9). SMIM based inversion quantifies abnormalities much more accurately than empirical second moments or visual inspection of propagators, and confirms the asymmetric trend observed by [7] in other porous media, in the quasi-asymptotic regime.

The parameter values found in the optimization procedure are also of interest (see the caption of Fig. 8). First, the velocity v in the SMIM model represents the average velocity of the water molecules while they are moving along mean flow direction, i.e. during a fraction of the total time equal to $1/(K+1)$. Indeed, the disordered time schedule of the MIM is quantified by parameters ω and K: the optimized K value of 0.05 suggests that longitudinal small-scale motions occupy $1/(K+1) = 95\%$ of the total time, while transverse motions and/or arrests representing 5%. The resulting average displacement by unit time is $\frac{v}{1+K} = 0.096 cm/s$, very close to the classical estimate $q/\Phi = 0.096 \pm 0.003 cm/s$ based on Darcy flow rate q and porosity Φ (average pore velocity).

Two phase flow- The SMIM model also mimics signals recorded in two phase flow conditions (in a water-oil mixture saturating the grain pack), for which classical analysis suggested strong dispersion. In this case, we analyze small-scale displacements of water wetting the grains, while oil is non wetting and not detected. Due to experimental constraints, the flow rate was limited to 50ml/h yielding an average pore velocity of 0.0175 cm/s, about 5 times smaller than in single phase flow conditions. Although the criterion for qualifying the dispersion regime has to be redefined to include the effect of saturation, the data analyzed here are most likely in an intermediate regime between pre-asymptotic and asymptotic. Nevertheless, we took 4 time intervals between 0.3s and 0.7s and found a much lower value of α (1.77), suggesting a super-dispersion effect. The quality of the fit is similarly very convincing (Fig. 10) although the minimum of the normalized objective function is higher (4.7). In this case, propagators are clearly non-symmetric, and this is well reproduced by the SMIM model at all times (Fig. 11). Beside a low value of α compared to single phase flow conditions, the parameter K increased considerably (0.74), meaning that the time spent not moving (in mean flow direction) is much larger. As a consequence,

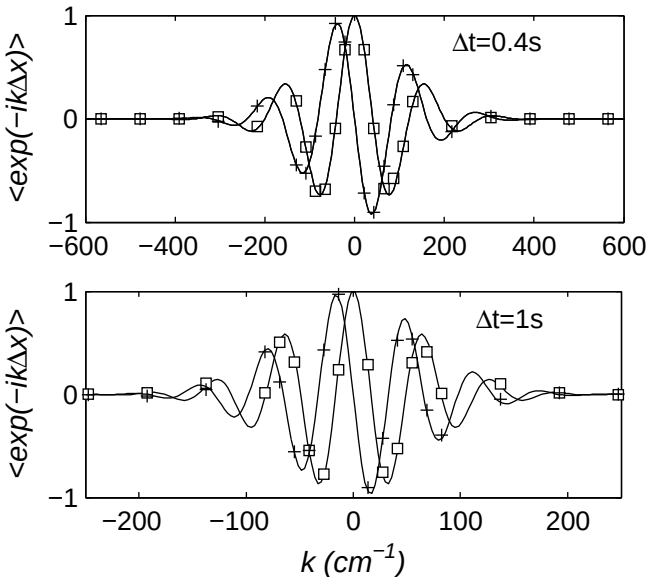

FIG. 8: Real and imaginary NMR signals (symbols), and best fit using NMR data collected at time intervals $\Delta t = 0.4, 0.5, 0.7, 0.8$ and $1s$. Only the data at 0.4 and $1s$ are shown. The sample is a $30\mu m$ grain pack in which water is flowing at a rate of $700ml/h$. For these conditions, a quasi-asymptotic dispersion regime is reached. The fitted parameters are: $v = 0.101cm/s$, $D = 1.50 \times 10^{-4} cm^{\alpha}/s$, $\omega = 10.4s^{-1}$, $K = 0.05$, $< M >= 0.57$, $\alpha = 1.91$.

the fitted average velocity while moving (0.033cm/s) is much larger than the average pore velocity (0.0175cm/s). This is in agreement with the intuitive idea that velocity contrast may increase when water saturation decreases.

V. CONCLUSION

We have illustrated how to combine the remarkable information of PFG NMR measurements with the analytical form (Eq.(8)) of the increment characteristic function of the SMIM in order to characterize the flow in a porous column in single and two phase flow conditions.

To this goal, we first investigated the increments of stochastic process SMIM that combines finite memory temporal disorder with dispersion or super-dispersion, i.e. two principles that separately allow non-symmetric propagators. This transport model is deduced from a stable process by imposing to each sample path a random time schedule composed of mobile steps alternating with immobile steps, all having random durations drawn from two expo-

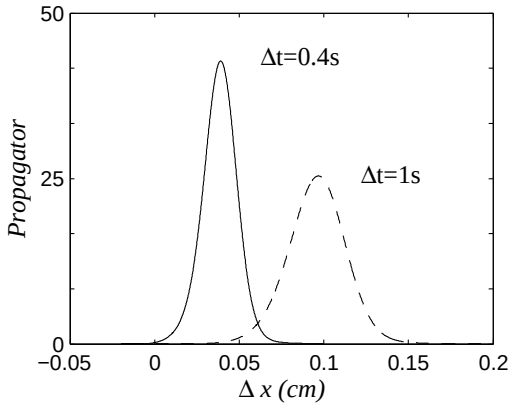

FIG. 9: Single phase flow propagators calculated from the SMIM model after fitting the NMR data presented in Fig. 8

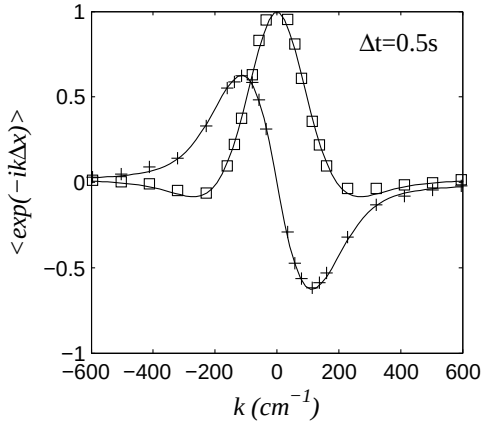

FIG. 10: Real and imaginary NMR signals (symbols), and best fit using NMR data collected at time intervals $\Delta t = 0.3, 0.4, 0.5$ and $0.7s$. Only the data at $0.5s$ are shown. The sample is a $30\mu m$ grain pack in which water and oil are flowing simultaneously (only the water signal is detected). The water saturation is 0.42. The fitted parameters are: $v = 0.033cm/s$, $D = 1.67 \times 10^{-4} cm^{\alpha}/s$, $\omega = 7.9s^{-1}$, $K = 0.74$, $< M >= 0.44$, $\alpha = 1.77$.

nential probability laws. As a result, the SMIM does not have the Markov property, hence its one-time distribution does not describe the statistics of its increments. Moreover, the SMIM includes stable variables more general than normal law to describe the amplitude of random motions. However, normal law is not excluded. This model has six parameters: the stability exponent α of the Lévy law, its skewness β that takes its maximum value of 1 on our

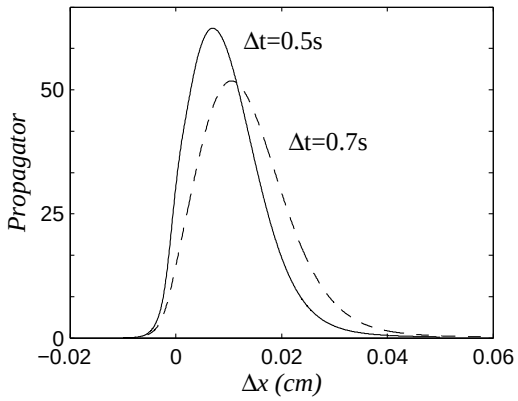

FIG. 11: Two-phase flow propagators calculated from the SMIM model after fitting the NMR data presented in Fig. 10.

data, the generalized dispersion coefficient D, the characteristic time $1/\omega$ of the exponential distribution describing the immobile time steps, the ratio K of average immobile and mobile times, and the average velocity of particles when they are moving. The auxiliary parameter $\mathcal{M}$ accounts for the distribution of the time that each particle has been following SMIM's time schedule when its displacement begins being measured. The analytical expression (8) has then been used to simultaneously analyze pulsed field gradient NMR signals acquired at different time intervals, with a robust parameter estimation based on standard optimization routine.

We were able to determine the appropriate (generalized) dispersion coefficients (D, v, α) as well as the parameters related to the classical MIM model (ω, K), often used to interpret tracer tests in soils or partially saturated media. In single phase flow conditions, we determine a stability exponent slightly different from 2 ($\alpha = 1.91$), for displacements long enough to belong to the quasi-asymptotic dispersion regime observed by [7], in agreement with the slight super-dispersion observed in [5]. Such small deviations might be hard to detect on displacement distributions (propagators), necessarily computed from measured characteristic functions [4]. In two phase flow conditions, the stability exponent deviates further from 2 ($\alpha = 1.77$), again in agreement with the strong super dispersion observed in [5].

APPENDIX A: MOLECULAR DISPLACEMENTS RECORDED BY NMR

Pulsed field gradient NMR is a non intrusive measurement technique that investigates molecular displacements in fluid flows, and is especially useful in porous materials. This non-intrusive technique enables the measurement of the characteristic function $\langle e^{-ik\Delta x}\rangle$ of the displacements of water molecules (described in details in the textbook [2]).

The porous media considered here is a long (30cm) sand pack column of uniform porosity placed in a NMR apparatus (Fig. 12 see also [5] for more details). The investigated volume is a (8 mm thick) slice $\mathcal{S}$ of the column, located at mid-height, far from inlet and outlet. It is submitted to a constant magnetic field of intensity B_0 in the $\vec{z}$ direction generated by two permanent magnets. A magnetization is created in $\mathcal{S}$ by sending a selective excitation pulse at the Larmor frequency (20 MHz), using the NMR antenna. After this pulse, the magnetization $\mathbf{M}$ in the sample is precessing around the direction $\vec{z}$ at the Larmor frequency. To encode the positions of the spin bearer molecules in a similar way as in imaging techniques, two opposite gradient pulses separated by a time interval Δt are used, such that the magnetic field seen by a water molecule during each gradient pulse at a location $\vec{r}$ is $B_0 + \vec{g}\cdot\vec{r}$. As a result, after the first pulse, the magnetization $\mathbf{M}$ has a phase encoding $\gamma d\vec{g}\cdot\vec{r}$ depending on location, where d and γ are the duration of the gradient pulse ($d << \Delta t$), and the proton giro magnetic ratio. For the same water molecule now at position $\vec{r}+\overrightarrow{\Delta r}$, the second (opposite) pulse generates a net phase change $-\gamma d\vec{g}\cdot\overrightarrow{\Delta r}$ depending on displacements Δr. In the present situation, the gradient direction is chosen parallel to the column axis in order to analyze the displacements of water molecules projected to the mean flow direction ($\vec{x}$). Noting $k = \gamma dg$ with g being the amplitude of the gradient pulse, the magnetization from all molecules present in the slice is then of the form of $\mathbf{M} = \mathbf{M}_0 e^{i\Phi_0}\langle e^{-ik\Delta x}\rangle$, where Δx is the displacement during the time interval Δt, in the $\vec{x}$ direction. In practice, the signal $\mathbf{M}$ is recorded for a set $\{k_n\}$ of k values at a fixed time interval Δt, and this is repeated for other values of Δt.

To compare the NMR data with models, the signal $\mathbf{M}$ is first normalized by $\mathbf{M}_0$, and then re-phased to yield $\langle e^{-ik\Delta x}\rangle$, a complex valued function of k and Δt whose real part is symmetric. We call $S(k_n^{(m)}, \Delta t_m)$ finite sequences of complex number $\langle e^{-ik_n^{(m)}\Delta x}\rangle$ at different Δt values: wave-numbers $k_n^{(m)}$ correspond to different $\Delta t^{(m)}$ Usually, about 40 $k_n^{(m)}$ values are used to sample the signal down to the noise level for each time interval Δt_m, typically

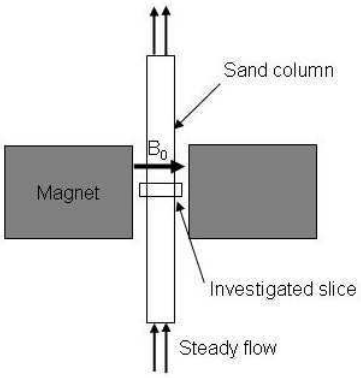

FIG. 12: NMR set-up for measuring water molecule displacements; a long plastic column (30 cm) that can be filled with sand is placed in the NMR apparatus comprising essentially two permanent magnets generating a permanent magnetic field B_0, and a NMR antenna (not shown). An imaging technique allows selecting a slice of thickness 8 mm within the column and far from the inlet/outlet, in which measurements are performed. The column allows injecting a steady flow of water from the bottom to the top.

varying between 0.1 and 1s (see details in [5]). Applying the inverse Fourier transform to each experimental series $S(k_n^{(m)}, \Delta t_m)$ returns tentative approximations to the p.d.f. of Δx, also called a propagator.

APPENDIX B: STABLE LÉVY LAWS

The shortest definition of standard Lévy variables $\mathcal{L}^{\alpha,\beta}$ [33–36] can be given in terms of their characteristic function

$$\langle e^{-ik\mathcal{L}^{\alpha,\beta}} \rangle = e^{-\varphi_{\alpha,\beta}(k)}, \tag{B1}$$

the Log-characteristic exponent being

$$\varphi_{\alpha,\beta}(k) = |k|^{\alpha}[1 + i\beta\tfrac{k}{|k|}\tan(\tfrac{\pi\alpha}{2})] \quad \text{for} \quad \alpha \neq 1. \tag{B2}$$

These Lévy variables are indexed by two parameters: the stability index α belongs to $]0, 2]$. It describes the asymptotic decrease of the density $\sim x^{-\alpha-1}$ (except for $x\beta < 0$ and $\beta = \pm 1$). The skewness parameter β ranges between -1 and 1. Fig. 13 demonstrates its influence, by comparing the p.d.fs of $\mathcal{L}^{\alpha,\beta}$ for $\beta = 0$ and $\beta = 1$. Large positive values are

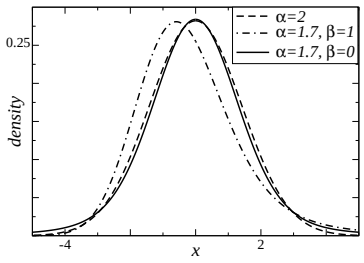

FIG. 13: Lévy variable densities. Lévy variables with $1 < \alpha < 2$ have p.d.fs that asymptotically decrease as powers, except in the maximally skewed case. For $\beta = 1$, the p.d.f. is proportional to $x^{-1-\alpha}$ at large positive x (as in the symmetric case), but decreases exponentially at large negative values (as for normal law).

enhanced by $\beta = 1$, large negative values are very rare in this case, as rare as for normal law. Yet, this is compensated by negatively pushing the most probable values.

APPENDIX C: FRACTIONAL DERIVATIVES

Riemann-Liouville derivatives $D^{\alpha}_{a,x}$ and $D^{\alpha}_{x,b}$ that appear in operator L and System (4) are defined by

$$D^{\alpha}_{a,x} f(x) = K^{+}_{\alpha} (\tfrac{d}{dx})^{\alpha''} \int_a^x \tfrac{f(y)}{(x-y)^{\alpha'}} dy,$$
$$D^{\alpha}_{x,b} f(x) = K^{-}_{\alpha} (\tfrac{d}{dx})^{\alpha''} \int_x^b \tfrac{f(y)}{(y-x)^{\alpha'}} dy$$

provided α is not an integer, with $K^{\pm}_{\alpha} = \frac{(\pm 1)^{[\alpha]+1}}{\Gamma([\alpha]+1-\alpha)}$, $\alpha'' = [\alpha] + 1$ and $\alpha' = \alpha - [\alpha]$ [37].

APPENDIX D: THE LAPLACE TRANSFORM OF THE INCREMENTS OF Z_t

Hitting times of general Lévy subordinators are studied in [30]: Z_t being the hitting time of the Lévy subordinator $T(z)$ of Laplace transform $\langle e^{-sT(z)} \rangle = e^{-z\psi(s)}$, the Laplace transform $f_{\omega,K}(\eta, t_1, \Delta t) = \langle e^{-\eta(Z_{t_1+\Delta t} - Z_{t_1})} \rangle$ is of the form of

$$\langle e^{-\eta(Z_{t_1+\Delta t} - Z_{t_1})} \rangle = 1 - \eta [R(t + t_1) * \mathcal{G}(t)](\Delta t), \tag{D1}$$

where function R is defined by its Laplace transform $1/\psi(s)$. Moreover, function $\mathcal{G}$ is $\mathcal{G}(t) = [\Sigma_{\geq 0} (-\eta)^n R^{n*}(\cdot) * 1](t)$, the superscript $n*$ representing n times iterated Laplace convolution, and in our case function ψ satisfies $\psi(s) = s(1 + \frac{K\omega}{\omega + s})$ (Eq. (15) of [11]). This

implies $R(t) = \frac{1}{K+1}[1 + Ke^{-\omega(K+1)t}]$, and

$$\mathcal{G}(t) = \frac{r_+ e^{tr_+} - r_- e^{tr_-}}{r_+ - r_-} + \frac{\omega(K+1)}{r_+ - r_-}[e^{tr_+} - e^{tr_-}].$$

The roots $r_\pm(\omega, K, \eta)$ of polynomial $s^2 + s[\eta + \omega(K+1)] + \eta\omega$ satisfy

$$r_\pm(\omega, K, \eta) = -\tfrac{1}{2}[\eta + \omega(K+1)] \pm \sqrt{\delta}(\omega, K, \eta), \tag{D2}$$

with

$$\delta(\omega, K, \eta) = (\eta + \omega(K+1))^2 - 4\eta\omega. \tag{D3}$$

Hence, the characteristic function (in Laplace form) of $Z_{t_1+\Delta t} - Z_{t_1}$ is

$$f_{\omega,K}(\eta, t_1, \Delta t) = \tfrac{\eta}{K+1}[(H_- + G\mathcal{M})e^{r_-\Delta t} - (H_+ + G\mathcal{M})e^{r_+\Delta t}], \tag{D4}$$

where we have set

$$\mathcal{M} = e^{-\omega(K+1)t_1}, \tag{D5}$$

with

$$\begin{array}{l} H_\pm(\omega, K, \eta) = \frac{A_\pm(\omega,K,\eta)}{r_\pm(\omega,K,\eta)} \\ A_\pm(\omega, K, \eta) = \frac{\omega(K+1)-\eta}{2\sqrt{\delta(\omega,K,\eta)}} \pm \frac{1}{2}, \end{array} \tag{D6}$$

and

$$G(\omega, K, \eta) = \frac{K}{\sqrt{\delta(\omega, K, \eta)}}. \tag{D7}$$

For $\frac{|\eta|}{\omega(K+1)} << 1$, Taylor expansion of D2-D7 implies $\frac{\eta}{K+1}H_+ \sim -1 + \frac{K\eta^2}{\omega^2(K+1)^4}$, $\frac{\eta}{K+1}H_- \sim \frac{K\eta^2}{(K+1)^2}$, and $G \sim -\frac{K}{\omega(K+1)}$. Hence, due to $0 < \mathcal{M} \leq 1$, $r_+ \sim -\frac{\eta}{K+1}$ and $r_- \sim -\omega(K+1)$, so that $-(H_+ + G\mathcal{M})\frac{\eta}{K+1}e^{r_+\Delta t}$ dominates the right hand-side of (6) when Δt is not too small.

Acknowledgments

The authors have been supported by Agence Nationale de la Recherche (ANR project ANR-09-SYSC-015)

Bibliography

[1] M. Sahimi, *Flow and transport in porous media and fractured rock* Wiley Vch: Weinheim (2011).

[2] P.T. Callaghan, *Principles of Nuclear Magnetic Resonance Microscopy* Clarendon press, Oxford (1991).

[3] B. Dybiec, E. Gudowska-Nowak, *Phys. Rev. E* **80**, 061122 (2009).

[4] U.M. Scheven, D. Verganelakis, R. Harris, M.L. Johns, and L.F. Gladden, *Physics of Fluids* **17**, 117107 (2005).

[5] V. Guillon, M. Fleury, D. Bauer, and M.C. Néel. *Phys. Rev. E* **87**, 043007 (2013).

[6] R.S. Maier, D.M. Kroll, R.S. Bernard, S.E. Howington, J.F. Peters, and H.T. Davis, *Physics of Fluids* **12**, 2065 (2000).

[7] U.M. Scheven, R. Harris, and M.L. Johns. *Phys. Rev. L.* **99**, 054502 (2007).

[8] J.H. Cushman, D. O'Malley, and Moongyu Park, *Phys. Rev. E* **79**, 032101 (2009).

[9] P. de Anna, T. Le Borgne, M. Dentz, A.M. Tartakovsky, D. Bolster and P. Davy. *Phys. Rev. L.* **110**, 184502 (2013).

[10] R. Schumer, D. A. Benson, M. M. Meerschaert, B.Baeumer, *Water Res. Research* 39 (10) (2003) 1296.

[11] D.A. Benson, and M.M. Meerschaert, *Adv. Water Resources* (32), pp 532-39 (2009).

[12] R. Gorenflo, F. Mainardi, and A. Vivoli, Chaos Solitons Fractals (34): 87 (2007).

[13] R. Metzler and J. Klafter, *J. Phys. A: Math. Gen.* **37**, R161-R208 (2004).

[14] R. Klages, G. Radons, and I.M. Sokolov Eds. *Anomalous transport, Foundations and Applications.* Wiley-VCH, Weinheim (2008).

[15] A. Valocchi, and H.A.M. Quinodoz, *Groundwater Contamination, IAHS Publ., L. M. Abriola Ed.* 185:35-42 (1989).

[16] H.A.M. Quinodoz, and A. Valocchi, *Water Resour. Res.* 29(9), 3227-3240 (1993).

[17] H.A. Deans, *Soc. Pet. Eng. J.* 3, 49 (1963).

[18] K.H. Coats, and B.D. Smith, *Soc. Rec. Eng. J.* 4, 73 (1964).

[19] L.E. Baker, *Soc. Pet. Eng. J.* 17, 319 (1977).

[20] E. Barkai and I.M. Sokolov, *J. Stat. Mech.* P08001 (2007).

[21] A.E. Kyprianou, *Introductory Lectures on Fluctuations of Lévy processes with Applications.* Universitext Springer, Heidelberg (2006).

[22] T. Le Borgne, M. Dentz, and J. Carrera. *Phys. Rev. E* **78**, 026308 (2008).

[23] T. Le Borgne, M. Dentz, and J. Carrera. *Phys. Rev. L.* **101**, 090601 (2008).

[24] A.M. Tartakovsky, D.M. Tartakovsky, and P. Meakin. *Phys. Rev. L.* **101**, 044502 (2008).

[25] M. Dentz, and D. Bolster. *Phys. Rev. L.* **105**, 244301 (2010).

[26] M. Dentz, T. Le Borgne, and J. Carrera. *Phys. Rev. E* **77**, 020101 (2008).

[27] B. Berkowitz, and H. Scher. *Phys. Rev. E* **57**, 5858 (1998).

[28] H. Scher,K. Willbrand, and B. Berkowitz. *Phys. Rev. E* **81**, 031102 (2010).

[29] M. Montero and J. Masoliver. *Phys. Rev. E* **76**, 061115 (2007).

[30] SH Rakotonasy,M.C. Néel, and M. Joelson, *Comm. Nonlin. Sci. Num. Simulat.*, 19, pp 2284-2293 (2014).

[31] M.C. Néel, S.H. Rakotonasy, D. Bauer, M. Joelson, and M. Fleury, *J. Stat. Mech.* P02006 (2011).

[32] See Matlab help on *fmincon* function.

[33] B. V. Gnedenko, and A. N. Kolmogorov, *Limit distributions for sums of independent variables*, Addison Wesley, Reading, MA, (1954).

[34] P. Lévy, *Théorie de l'addition des variables aléatoires* Gauthier-Villars, Paris(1937).

[35] W. Feller, *An Introduction to Probability Theory and its Applications*, vol. II Wiley, New York (1970).

[36] R. Weron, *Stat. Prob. Lett.* 28, 165-71 (1996).

[37] S.G. Samko, A.A. Kilbas, and O.I. Marichev, *Fractional integrals and derivatives: theory and applications* Gordon and Breach, New York (1993).